

PPPL-2255

PPPL-2255

UC20-F,G

209
3/11/86

M.L.R. (2)
(25)


DR-1589-X

HEAT PULSE PROPAGATION STUDIES IN TFTR

By

E.D. Fredrickson et al.

FEBRUARY 1986

PLASMA
PHYSICS
LABORATORY 

DISTRIBUTION OF THIS DOCUMENT IS UNLIMITED

PRINCETON UNIVERSITY
PRINCETON, NEW JERSEY

PREPARED FOR THE U.S. DEPARTMENT OF ENERGY,
UNDER CONTRACT DE-AC02-76-CED-3073.

DISCLAIMER

This report was prepared as an account of work sponsored by an agency of the United States Government. Neither the United States Government nor any agency thereof, nor any of their employees, makes any warranty, express or implied, or assumes any legal liability or responsibility for the accuracy, completeness, or usefulness of any information, apparatus, product, or process disclosed, or represents that its use would not infringe privately owned rights. Reference herein to any specific commercial product, process, or service by trade name, trademark, manufacturer, or otherwise does not necessarily constitute or imply its endorsement, recommendation, or favoring by the United States Government or any agency thereof. The views and opinions of authors expressed herein do not necessarily state or reflect those of the United States Government or any agency thereof.

HEAT PULSE PROPAGATION STUDIES IN TFTR

E. D. Fredrickson, J. D. Callen¹, K. McGuire, J. D. Bell², R. J. Colchin²,
 P. C. Efthimion, K. W. Hill, R. Izzo, D. R. Mikkelsen, D. A. Monticello,
 V. Pare², G. Taylor, and M. Zarnstorff

Plasma Physics Laboratory

PPPL--2255

Princeton University

DE86 007532

Princeton, NJ 08544

ABSTRACT

The time scales for sawtooth repetition and heat pulse propagation are much longer (10's of msec) in the large tokamak TFTR than in previous, smaller tokamaks. This extended time scale coupled with more detailed diagnostics has led us to revisit the analysis of the heat pulse propagation as a method to determine the electron heat diffusivity, χ_e , in the plasma. A combination of analytic and computer solutions of the electron heat diffusion equation are used to clarify previous work and develop new methods for determining χ_e . Direct comparison of the predicted heat pulses with soft X-ray and ECE data indicates that the space-time evolution is diffusive. However, the χ_e determined from heat pulse propagation usually exceeds that determined from background plasma power balance considerations by a factor ranging from 2 to 10. Some hypotheses for resolving this discrepancy are discussed.

DISTRIBUTION OF THIS FILE IS UNLIMITED

¹University of Wisconsin, Madison, Wisconsin.

²Oak Ridge National Laboratory, Oak Ridge, Tennessee.

MASTER

I. INTRODUCTION

The dominant energy loss mechanism in large tokamaks such as TFTR [1] is generally thought to be due to anomalous electron heat conduction, and is usually characterized by scaling laws for the global energy confinement time τ_E . However, few methods have been available to measure directly the local electron heat conduction. Work in this area started in 1975, in the FM-1 Spherator [2]; application to tokamaks using the naturally occurring sawtooth oscillations in ORMAK as the source of heat pulses was first discussed by Callen and Jahns [3]. More detailed analyses of the "small signal response" heat pulse propagation problem [4] were used to obtain values of the electron heat diffusivity χ_e in ORMAK which were in reasonable agreement with those obtained through power balance, or global energy confinement calculations. A number of new methods for determining χ_e from sawtooth-induced electron heat redistributions were discussed in a paper by Soler and Callen [5]. This paper explains in detail many useful techniques for inferring χ_e from experimental observations of the space-time evolution of the electron temperature perturbations and serves as the starting point for this paper. The most comprehensive use of the heat pulse propagation technique to date was that by Bell *et al.* [6] who showed that in ISX-B the χ_e increases as the neutral beam heating power is increased, in reasonable accord with the observed L-mode degradation in τ_E [7]. Reference 6 also includes, for the first time, the soft X-ray chord-averaging effects, at least numerically. Recently, pulsed electron cyclotron heating has been used in D-III to induce heat pulses whose propagation is followed by a new temporal Fourier analysis technique [8], a variation of which will be discussed below.

In ohmic-heated and neutral-beam-heated TFTR discharges the characteristic time scales for sawtooth oscillations have been found to be

much longer than in previous, smaller tokamaks, with the sawtooth periods extending up to 50 msec [1]. In addition, the time scale for the peak of the outwardly propagating heat pulse to reach the plasma edge ranges up to about 30 msec. These greatly extended time scales, and the availability of fast time scale local electron cyclotron emission (ECE) measurements of T_e as well as an extensive soft X-ray imaging system have led us to revisit and substantially extend the previous work [3-6] on determining χ_e from the propagation of the sawtooth-induced heat pulse.

In Sec. II of this paper we review previously developed methods for determining χ_e from heat pulse propagation, rectify some previous errors, and introduce some new methods for determining χ_e . Throughout this section TFTR experimental data are utilized to demonstrate the different analysis techniques. Next, in Sec. III we investigate with computational models the sensitivity of the various types of analysis to the simplifying assumptions used in Sec. II (delta function source, density and χ_e radial profiles, chord averaging, etc.). In Sec. IV we discuss the χ_e results obtained under a variety of experimental conditions in TFTR and compare these results with those obtained from power balance considerations. Since the χ_e 's determined from heat pulse propagation substantially exceed those determined from the power balance for the background plasma, in Sec. V we discuss some hypotheses for resolving this discrepancy.

II. HEAT PULSE PROPAGATION ANALYSIS

Following the work of Soler and Callen [5], a mathematical description of the heat pulse propagation problem is provided beginning from the general electron heat balance equation:

$$\frac{3}{2} n_e(r) \frac{\partial T_e(r,t)}{\partial t} = \frac{1}{r} \frac{\partial}{\partial r} \left[r n_e(r) \chi_e(r) \frac{\partial T_e(r,t)}{\partial r} \right] + \Sigma Q, \quad (1)$$

where ΣQ represents all electron heat sources and sinks such as ohmic heating, collisional heat transfer to ions, convection, radiation, auxiliary heating, etc. A small, sawtooth-induced electron temperature perturbation $\tilde{T}(r,t)$ of a near-equilibrium situation is governed by the equation:

$$\frac{3}{2} n_e \frac{\partial \tilde{T}(r,t)}{\partial t} = \frac{1}{r} \frac{\partial}{\partial r} \left[r n_e \chi_e \frac{\partial \tilde{T}(r,t)}{\partial r} \right]. \quad (2)$$

This equation is derived by perturbing Eq. (1) and neglecting the additional term $\tilde{T} \partial (\Sigma Q) / \partial T \sim -n \tilde{T} / \tau_E$ because the equilibrium evolution implied by this term is slow and broadly distributed relative to the highly localized (in space and time) perturbations $\tilde{T}(r,t)$ induced by the sawteeth. (Additional electron heat sources which arise from the residual kinetic energy in plasma flows and magnetic fluctuations just after a sawtooth "crash" are discussed in Appendix A and shown to be negligible.)

The physical situation we wish to model is illustrated in Fig. 1. An analytic solution of Eq. (2) for $\tilde{T}(r,t)$ with a temperature perturbation initial condition given by the sum of two opposing delta functions ("dipole" heat source) was obtained by Soler and Callen [5] through a Green's function solution of the basic heat diffusion equation:

$$\tilde{T}(r,t) = \frac{A^2 r_1 r_2}{2t} e^{-A^2 r^2 / 4t} \left[e^{-A^2 r_2^2 / 4t} I_0\left(\frac{A^2 r r_2}{2t}\right) - e^{-A^2 r_1^2 / 4t} I_0\left(\frac{A^2 r r_1}{2t}\right) \right]$$

(3)

where t is the time measured from the sawtooth crash time t_0 , $A^2 = 3/2\chi_e$, r_s is the inversion ($q = 1$) radius, r_0 ($\lesssim \sqrt{2} r_s$) is the reconnection radius and r_1 ($0 < r_1 < r_s$) and r_2 ($r_s < r_2 < r_0$) are the positions of the assumed negative and positive delta function temperature perturbations of magnitude \tilde{T}_0 . (For no net heat input but only energy redistribution from the sawtooth crash phase we must have $\int r dr \tilde{T}(r, t = 0) = 0$, which indicates that $-r_1 \tilde{T}_1 = r_2 \tilde{T}_2 \equiv r_1 \tilde{T}_0$.) A long time (small Bessel function argument), asymptotic expansion of Eq. (3) obtained in Ref. 5 can be written as $\tilde{T}(r, t) \sim (r^2/t^3) \exp(-A^2 r^2/4t)$, which indicates the maximum temperature perturbation at a given radius r occurs at the time $t_p = A^2 r^2/12 = r^2/8\chi_e$ with a magnitude $\tilde{T}(r, t_p)$ falling off as r^{-4} . While these results are physically appealing (i.e., $t_p \sim r^2$, consistent with a diffusion process), they do not represent a self-consistent solution in that the argument of the Bessel functions ($-6r_s/r > 1$) is large, not small at the time $t = t_p$. (The range of r/r_s , which is of interest, is $2 \lesssim r/r_s \lesssim 5$ since for $r/r_s < 2$ the heat pulse shapes can depend too critically upon the initial conditions, while for $r/r_s > 5$ the temperature perturbations become negligible in amplitude because of the r^{-4} magnitude scaling.)

To develop an approximate formula for $\tilde{T}(r, t)$ from Eq. (3) that is valid around the temporal peak in \tilde{T} , we make a large argument expansion of the Bessel functions using $I_0(z) \sim e^z/\sqrt{2\pi z}$. Then, expanding $(r_1/r_2)^{1/4} = 1 - (r_2 - r_1)/4r_s + \dots$, and assuming $A^2 r(r_2 - r_s)/2t \ll 1$ and $A^2 r(r_s - r_1)/2t \ll 1$, we find to lowest order

$$\tilde{T}(r, t) = \tilde{T}_0 \frac{A^3 r_s r_1 (r_2 - r_1)}{4\sqrt{\pi} (r_1 r_2)^{1/4}} \left[\frac{\sqrt{re^{-A^2(r-r_s)^2/4t}}}{t^{3/2}} \right] \left[1 - \frac{t}{A^2 r_s} \right] \quad (4)$$

The primary assumptions under which this equation was derived and which are tested numerically below are:

- 1) That the initial temperature perturbation can be described by the sum of an outer ($r = r_2$) positive delta function and an inner ($r = r_1$) negative delta function, the volume integral of which gives no heat input.
- 2) That the density n and electron heat diffusivity χ_e are constant in radius.

Setting the time derivative of Eq. (4) to zero, we find the time t_p at which the peak of $\tilde{T}(t)$ occurs is given, to lowest order, by

$$t_p = \frac{A^2(r - r_s)^2}{6 + (r - r_s)^2/rr_s} = \frac{3(r - r_s)^2/2 \chi_e}{6 + (r - r_s)^2/rr_s} \quad (5)$$

At the time $t = t_p$ the argument of the Bessel functions is larger than unity for the range of r/r_s values of interest, so this solution is self-consistent. While the scaling of t_p with r is not so obvious from Eq. (5), the derivative dt_p/dr^2 is equal to $A^2/13.5$ to within 7% for $1.7 < r/r_s < 5$, which covers the radial range of interest. Thus, we expect the change in t_p as r^2 increases to be given by

$$\Delta t_p = \frac{\Delta r^2}{13.5 A^2} = \frac{\Delta r^2}{9\chi_e} \quad (6)$$

Hence, if a plot is made of t_p versus r^2 the data should fall on a straight line whose slope is $1/9\chi_e$. This was the original technique used [3-5] to

infer x_e from heat pulse propagation data, although historically the coefficient of $1/8$ obtained in Ref. 5 has been used. Since the coefficient differs by only about 10%, we will also use $1/8x_e$ for simplicity in the remainder of this paper.

Two examples of experimental data from TFTR that are utilized to determine x_e from heat pulse propagation are shown in Figs. 2 and 3. Figure 2 shows the propagation of a heat pulse from the crash of a typical sawtooth. Figure 3 shows the much slower propagation of a heat pulse that is sometimes seen resulting from the first sawtooth crash (the "event") during a discharge. A plot of t_p versus r^2 for this data is shown in Fig. 4, from which it is readily apparent that t_p increases roughly linearly with r^2 , consistent with Eq. (6). The difference in the heat pulse propagation between the "event" and typical sawteeth will be discussed in Sec. V.

As a check on the diffusive nature of the heat pulse propagation, we can also compare the pulse shapes in time with the time-dependent part of Eq. (4) which, neglecting the small $t/(A^2 r r_s)$ term, can be written in a normalized form as

$$f(t) \equiv \frac{\tilde{T}(r, t)}{\tilde{T}(r, t_p)} = \frac{\exp \left[+ \frac{3}{2} \left(1 - \frac{t}{t_p} \right) \right]}{(t/t_p)^{3/2}} \quad (7)$$

Since this temporal behavior could be modified by the chord-averaging effects of the soft X-ray diagnostics, we use the electron cyclotron emission (ECE) spectrometer measurement of the electron temperature (~ 5 cm radial and azimuthal resolution) for comparison with this theoretical prediction. An example of such a comparison is shown in Fig. 5, which indicates the pulse shape is reasonably close to that predicted. Note also that if, from other information, we know the singular or inversion radius r_s , then we can estimate

χ_e^{HP} from Eq. (5) using the t_p which gives the best fit of Eq. (7) to the temporal pulse shape. For the case shown we find $\chi_e^{\text{HP}} = 2.3 \times 10^4 \text{ cm}^2/\text{sec}$.

Since $f(t)$ is only a function of t/t_p , we would expect the times required for the decay of the pulses from their maxima $\tilde{T}(r, t_p)$ to fractional values thereof to just be some multiple of t_p . This behavior is illustrated in Fig. 6. Experimentally, the peak of the heat pulse is often very difficult to measure because of the short time delays involved, precursor oscillations, and finite sawtooth crash times. Thus, it is often useful to measure, say, the time for the pulse to decay to half maximum ($t_{0.5}$) and use this to estimate χ_e . An example of this procedure is shown in Fig. 7, which also shows that the ECE and soft X-ray data give approximately the same results. However, this method can be subject to inaccuracies due to soft X-ray chord-averaging effects and multiple pulses (discussed in Sec. III) since then the temporal pulse shapes can become distorted by a sort of pulse pileup effect. Generally speaking, since $\tilde{T}_e(r, t)$ for any given pulse decays for large t as $(t_p/t)^{3/2}$, as long as t_p is less than one quarter of the sawtooth repetition time τ_{saw} , the multiple pulse distortions of a given pulse by all of the preceding pulses are less than 15% in magnitude.

A further check on the diffusive character of the heat pulses is the rate of decrease with radius r of the maximum of the temperature perturbation. That is, the scaling of $\tilde{T}(r, t)$ evaluated at $t = t_p$:

$$\tilde{T}(r, t_p) = T_0 \frac{[r_1(r_2 - r_1)/r_s^2]}{4\sqrt{\pi} (r_1 r_s / r_s^2)^{1/4}} R(r/r_s) f(t/t_p)$$

in which

$$R(r/r_s) = \frac{\exp \left[-\frac{1}{4} (r - r_s)^2 / r r_s \right]}{(r/r_s) \left[((r - r_s)^2 / r r_s) / (6 + (r - r_s)^2 / r r_s) \right]^{3/2}} \quad (8)$$

While the radial dependence of $R(r/r_s)$ is quite complicated, over the radial range of interest ($2 < r/r_s < 5$) it is given approximately (to within 25%) by $260/(r/r_s)^4 \approx r^{-4}$, which has the same scaling with r as that indicated by the work in Ref. 5 [see discussion after Eq. (3) above]. A comparison between the predicted r^{-4} scaling and experimental data from ECE measurements of $\tilde{T}_e(r, t_p)$ is shown in Fig. 8. The agreement seems reasonable even though most of the available data are fairly close to the inversion radius ($r/r_s < 2$).

For plasmas with sawtooth oscillations that are periodic in time with a well-defined repetition time (the sawtooth period, τ_{saw}), the problems of pulse pileup and exact source function can be avoided through a phase shift analysis of the pulses based upon a Fourier analysis in time (cf. reference 8). In this approach we return to Eq. (2) and expand \tilde{T} in the Fourier series $\tilde{T}(r, t) = \sum_n \tilde{T}_n(r) \exp(in\omega t)$ with $\omega \equiv 2\pi/\tau_{\text{saw}}$. The Fourier harmonics $\tilde{T}_n(r)$ are governed by the differential equation (for n_e, χ_e assumed constant)

$$\left[r^2 \frac{\partial^2}{\partial r^2} + \frac{1}{r} \frac{\partial}{\partial r} - \left(\frac{3in\omega}{2\chi_e} \right) r^2 \right] \tilde{T}_n(r) = 0 . \quad (9)$$

Solutions of this equation are zero-order Kelvin (Bessel) functions of argument $x \equiv (3n\omega/2\chi_e)^{1/2} r$. Eliminating the solutions which are singular at $r = 0$ and taking a large r (or x) limit, we find

$$\tilde{T}_n(r) = C J_0(x e^{3i\pi/4}) = C(\text{ber}(x) + i \text{bei}(x)) = M(x) e^{i\psi(x)}$$

in which the phase $\psi(r)$ is given to lowest order by

$$\psi_n = \left(\frac{3n\omega}{4\chi_e} \right)^{1/2} r .$$

This phase increases linearly with r with slope $d\psi_n/dr = (3n\omega/4x_e)^{1/2}$ as long as $r > (x_e/3n\omega)^{1/2}$, which since empirically $\tau_{saw} \sim \tau_E/5 \sim a^2/20x_e$ becomes $r \geq a/20\sqrt{n}$, with a being the limiter radius. A second condition is that $r > r_0$, as the behavior within the reconnection region is not strictly diffusive. In this limit the cylindrical geometry has effectively been reduced to a slab geometry and the x_e can be estimated from

$$x_e = \frac{3n\omega}{4} \left(\frac{d\psi_n}{dr} \right)^{-2} \quad (10)$$

This method of analyzing heat pulse data can be readily automated, is independent of any specific model for the origin of the heat pulse, and automatically includes any distortions related to multiple heat pulses. (In contrast, the time to peak and pulse shape analysis can be affected by a pulse pileup type of effect with multiple pulses.) To obtain x_e between any two points in radius one determines the phase shift \tilde{T}_n for the heat pulses between the two radii and uses this result in Eq. (10). An illustration of this approach for TFTR heat pulses measured with the soft X-ray array is shown in Figs. 9 and 10. Since this technique is to some degree sensitive to the shape of the heat pulse, chord averaging effects could be important; and when used with soft X-ray arrays, there is the question of whether the soft X-ray signal is a close representation of the electron temperature. In this regard it is encouraging to note that the higher harmonic components (which are more sensitive to the pulse shapes) shown in Fig. 11 yield approximately the same x_e . Also, on TFTR comparison of the soft X-ray time to peak analysis with that obtained from the temperature pulses measured with the ECE spectrometer shows good agreement. The major drawback of this approach is the dependence

of x_e on the square of the slope of the phase shift. Of lesser importance is the necessity to analyze similar heat pulses in a nearly metronomic sequence to justify the Fourier analysis in time.

III. SENSITIVITY ANALYSIS

In order to study the sensitivity of the procedures developed in the preceding section to the assumptions used to derive them, we want to develop more general solutions of Eq. (2) for varying n_e , x_e , and initial conditions. Closed form analytic solutions for this general one-dimensional diffusion equation with variable coefficients are difficult to obtain [9]. However, numerical solutions are readily obtainable. For our numerical algorithm we integrate Eq. (2) using a fully implicit finite difference scheme which is first order accurate with respect to Δt and second order accurate with respect to Δr ;

$$\frac{3}{2} n_j \frac{T_j^{1+1} - T_j^1}{\Delta t} = \frac{1}{r_j \Delta r} \left\{ (rn\chi)_{j+1/2} \left(\frac{T_{j+1}^{1+1} - T_j^{1-1}}{\Delta r} \right) - (rn\chi)_{j-1/2} \left(\frac{T_j^{1+1} - T_{j-1}^{1-1}}{\Delta r} \right) \right\}$$

where

$$(rn\chi)_{j\pm 1/2} = \frac{1}{2} (r_j n_j \chi_j + r_{j\pm 1} n_{j\pm 1} \chi_{j\pm 1})$$

For each case reported below, convergence studies have been performed whereby Δr and Δt are independently reduced until there are no discernible changes in the solution. While such limits vary from case to case, typically $5 \times 10^{-3} \geq \Delta r/a \geq 10^{-3}$, $10^{-4} \geq \Delta t/(3a^2/2\chi_0) \geq 5 \times 10^{-6}$ in which a is the plasma radius and χ_0 is the electron heat diffusivity at the plasma center. Numerical effects are filtered out of the data presented below. As expected, for

regions $r_0 < r < 0.7a$ sufficiently far from the boundaries, the solutions were independent of the boundary conditions chosen. For simplicity, all of the numerical results presented below were carried out with $r_0/a = 0.2$ and Dirichlet boundary conditions.

We now utilize these numerical solutions to explore the sensitivity of the heat pulse characterizations given in Eqs. (3) - (8) to the assumptions used to derive them. First, we investigate the effects of different initial conditions. An experimental estimate obtained from ECE data is shown in Fig. 12. Taking n and χ to be constant in radius, but using various initial conditions, we find some modest variation of the numerically calculated t_p with r^2 , as indicated in Fig. 13. As could be anticipated, the effects of the varying initial conditions (much beyond the range of experimentally expected possibilities) are small and only important in the "near-field" region $r^2 < 2r_0^2$. The asymptotic region ($r > \sqrt{2}r_0$) is not significantly affected by these variations. The saturation of t_p with r^2 for $r^2 > 0.7a^2$ is due to "reflection" of the heat pulses from the boundary at $r = a$.

Next, we consider the effects of spatially varying n and χ_e profiles. The sensitivities here can be exhibited by writing Eq. (2) in the form:

$$\frac{3}{2} \frac{\partial \tilde{T}}{\partial t} = \frac{1}{r} \frac{\partial}{\partial r} r \chi_e \frac{\partial \tilde{T}}{\partial r} + \left(\frac{\partial \ln n}{\partial r} \right) \chi_e \frac{\partial \tilde{T}}{\partial r} \quad (11)$$

Thus, because of both the strong radial localization of the perturbations and the "weak" logarithmic dependence on $n(r)$, particularly for n decreasing as r increases, the solutions should depend only weakly on the density profile $n(r)$. The weakness of this profile effect is illustrated in Fig. 14 where t_p is plotted versus r^2 for some physically reasonable density profiles.

However, as can be anticipated from the form of Eq. (11), variations in the x_e profile can have significant effects. These are illustrated in Fig. 15. Here, we see that while t_p still varies roughly linearly with r^2 over the radial range of interest ($0.2^2 < r^2/a^2 < 0.8^2$), the slope does vary somewhat. A decreasing $x(r)$ has the clearly observable effect of causing t_p to increase faster than r^2 . Conversely, the normally expected case with a x_e increasing with radius decreases the slope of t_p versus r^2 , and causes t_p to increase less rapidly than r^2 for $r^2/a^2 \geq 0.6^2$. The decrease in the slope just indicates that the average x_e over the important range ($0.2^2 < r^2/a^2 < 0.6^2$) is higher than the value of x_e at $r = 0$, as indicated in Table I. As can be seen, the average x_e values inferred from the t_p versus r^2 data agree reasonably well with the simple cylindrical volume average of $x_e(r)$ defined by

$$\bar{x} \equiv (r_2^2 - r_1^2)^{-1} \int_{r_1}^{r_2} 2r dr x_e(r)$$

Thus, variations in the magnitude of x_e with plasma parameters should be discernable from experimental plots of t_p versus r^2 . Deviations of t_p from a linear scaling with r^2 for $0.6^2 < r^2/a^2 < 0.8^2$ in Fig. 15 indicate whether $x_e(r)$ increases or decreases with r . However, these deviations are relatively small and so it is difficult to extract directly the radial profile of x_e from experimental t_p versus r^2 data, particularly considering the likely experimental uncertainties.

As another check on the theoretical predictions, we have also used the code developed in Ref. 6 to investigate the variation of t_p with r^2 , including pulse "pileup." The pulse pileup effects are shown in Fig. 16 where the t_p versus r^2 curves are shown for the first and subsequent pulses for a case in which $x_e = 8 \times 10^3$ cm²/sec and the sawtooth period is relatively short ($\tau_{\text{saw}} =$

25 msec). In this relatively extreme case the χ_e determined from Eq. (6) increases by only about a factor of 2 in going from the first to the time asymptotic pulse. The variation becomes even smaller if we restrict the data to values of t_p less than $\tau_{\text{SAW}}/2$.

The sawtooth-induced heat pulses are often observed on TFTR through soft X-ray arrays which measure the radiation emitted above some cutoff energy (typically ~ 3 keV in TFTR). However, these arrays observe the emission integrated (or averaged) over chords through the plasma. Also, the soft X-ray emission per unit volume by photons with energies above the cutoff is not simply a measure of T_e . It can be written in the form $C n_e^2 T_e^\alpha$, where α is a coefficient which is typically 2.0 but can be as large as 5-10 near the low temperature ($\lesssim 100$ eV) edge of the plasma. To calculate the line-integrated emission and fluctuations in it due to the sawteeth, we need detailed temperature, density, and impurity profiles. This was done for ISX-B data in Ref. 6, but has not been done for TFTR data. To avoid possible problems due to the chord-averaging and detector response effects, we restrict our attention to the heat pulse shapes around their peaks, which are not strongly sensitive to these effects. Also, as indicated in Fig. 7, we often cross-check the results with the ECE-measured electron temperature fluctuations which are not influenced by these effects.

Finally, we note that while most of the preceding sensitivity analysis has concentrated on the t_p versus r^2 method of determining χ_e , the general conclusions derived also mostly apply to the phase shift analysis [cf. Eq. (10)]. This is because the phase shift type analysis also relies upon the diffusive nature of the heat pulse propagation over the radial range of interest. Thus, we can also expect the phase shift analysis to be relatively insensitive to density profile and chord-averaging effects (at least for low

harmonics of the basic frequency), and to be independent of pulse pileup effects and initial conditions (for the reasons stated previously). It will be sensitive to a χ_e varying with radius. In fact, if the experimental data is of high enough quality (low signal-to-noise ratio, metronomically repetitive, etc.), it may be possible to infer the radial dependence of χ_e from the use of Eq. (10) between successive radii in the plasma (c.f. Fig. 10).

IV. EXPERIMENTAL RESULTS FOR ELECTRON HEAT DIFFUSIVITY χ_e

In the preceding two sections we have shown that the sawtooth-induced heat pulse propagation can be described quite well by formulae derived from a diffusion equation for the electron heat diffusivity and that the χ_e so determined is not sensitively dependent on our simplifying assumptions. Analysis of experimental data by the various methods described in Sec. II have yielded electron heat diffusivity coefficients substantially larger than those obtained from power balance analysis (c.f. Figs. 2-5, 7, 9, 10).

In Fig. 17 the χ_e^{HP} determined for a wide range of plasma parameters is plotted against the χ_e determined from a power balance analysis. The data were analyzed using the phase shift method on small or simple (not compound) sawteeth. Since the discrepancy between the χ_e 's is so large, a natural question which arises is: under what conditions do they become closer and do they ever become the same. In looking over the experimental data base, as exemplified by the data presented so far, the cases which come the closest are those due to the first sawtooth crash (the "event") as indicated in Figs. 2-3. However, even there $\chi_e^{HP}/\chi_e^{PB} = 1.5$. Further, in Fig. 18 we show the evolution of the heat pulses as time progresses and successive sawteeth occur. As can be seen, while the "event," which occurs at about 1.75 seconds,

has a relatively slowly diffusing heat pulse, successive sawteeth, with increasing radii for the $q = 1$ surface, get progressively faster with shorter time delays, until the χ_e^{HP} increases by a factor of 4 or more for the 4th and successive heat pulses. Note from Fig. 16 that multiple-pulse effects can be at most a factor of 2. Thus, it appears that χ_e^{HP} increases substantially between 1.7 and 2.0 seconds in this TFTR discharge.

V. DISCUSSION AND CONCLUSION

In this paper we have shown that the electron heat pulses induced by the sawtooth crashes in TFTR propagate in a way that can be described by a diffusion equation [Eq. (2)]. Thus, while we cannot exclude other, more complex behavior, we can describe the heat pulse behavior as diffusive. Both ECE (local) and soft X-ray (chord-average) diagnostics have been utilized. The heat pulses have been shown to be diffusive on scale lengths of the order of the detector array spacings (~ 5 cm) through their: 1) diffusive propagation ($t_p \propto r^2$ in Figs. 4, 7, 14, 16); 2) pulse shapes in time (Fig. 4); and 3) decreasing magnitude with increasing radius (Fig. 7). However, the χ_e^{HP} characterizing this electron heat transport process in TFTR usually exceeds the χ_e^{PB} for the background plasma determined from power balance considerations. Most fundamentally, the heat pulses seem to diffuse much faster through the plasma than would be anticipated given the energy confinement time of these TFTR ohmic discharges ($\tau_E \sim 100 - 400$ msec).

As a comprehensive test to try to resolve this discrepancy in the magnitude of χ_e , we have simulated the sawteeth and concomitant heat pulses with the BALDUR transport simulation code. This code simulates sawteeth by flattening T_e and n_e , and changing J according to a Kadomtsev type flux reconnection model at fixed time intervals. Some example heat pulses obtained

from this transport simulation are shown in Fig. 19. Analyzing the t_p versus r^2 characteristics and other properties of these transport simulation heat pulses, we find that the χ_e we determine is within a factor of about 1.5 of the value of χ_e put into the code. Thus, even this check indicates that the heat pulses diffuse much more rapidly than would be expected on the basis of the (anomalous) background electron heat transport.

For a brief review of heat pulse propagation studies in other, smaller tokamaks, we note that χ_e^{HP} was of order χ_e^{PB} in ORMAK^{4,5} and ISX-B.⁶ However, in the somewhat larger D-III experiment a repetitively pulsed electron cyclotron heating experiment found⁸ $\chi_e^{\text{HP}}/\chi_e^{\text{PB}} \sim 2-4$. Also, in unpublished work, some other tokamak experiments have often measured heat pulses that seemed to propagate quite quickly. In addition to these comments, we should note that χ_e^{HP} has always been found to be in the range above 10^4 cm²/sec. In the previous, smaller experiments χ_e^{PB} was also usually larger than 10^4 cm²/sec so the two could agree. However, in TFTR the χ_e^{PB} values can go down to 3×10^3 cm²/sec or lower, but the χ_e^{HP} values seem to remain above 10^4 cm²/sec, thus leading to the discrepancies we find between χ_e^{PB} and χ_e^{HP} .

In trying to reconcile this discrepancy we have identified two different hypotheses for understanding why $\chi_e^{\text{HP}} \gg \chi_e^{\text{PB}}$:

- 1) The electron heat diffusivity χ_e varies during the time the heat pulses pass through the plasma. That is, we would have $\chi_e = \chi_e^{\text{PB}} + \tilde{\chi}_e$ where $\tilde{\chi}_e$ would only have to be a factor of 2-3 larger than χ_e^{PB} , but would vary rapidly in time. Note that with this form of χ_e the perturbed electron heat transport equation now includes a term of the form $1/r \partial/\partial r (r n_e \tilde{\chi}_e dT_{e0}/dr)$. The $\tilde{\chi}_e$ operates on the background electron temperature gradient and this can create an

effect similar to a heat pulse. As this hypothetical $\tilde{\chi}_e$ can change arbitrarily fast, the resulting "heat pulse" may also propagate at any chosen speed. A problem is that for an arbitrarily chosen $\tilde{\chi}_e(r,t)$, the resulting "heat pulse" will not look diffusive. The form of the additional term in the heat equation, however, suggests a $\tilde{\chi}_e(r,t)$ which will result in a "diffusive" heat pulse, that is that $\tilde{\chi}_e(r,t)$ is proportional to the gradient of the electron temperature, $\tilde{\chi}_e(r,t) \sim [(\partial T_e/\partial r)/(\partial T_{e0}/\partial r)]^B$ or with a small perturbation expansion $\tilde{\chi}_e \sim \beta (\partial T_e/\partial r)/(\partial T_{e0}/\partial r)$. Then $\beta = (\chi_e^{HP}/\chi_e^{PB}) = 1$, which is of order 2 - 10 for most TFTR data. Of course other forms of $\tilde{\chi}_e(r,t)$ might yield "heat pulses" similar enough to those expected from a purely diffusive process so that they would be experimentally indistinguishable.

- (2) A "heat pinch" [10]. Here we suppose that $\chi_e = \chi_e^{HP}$, but that there is an inward pinch term so that the electron heat transport equation has the form

$$\frac{3}{2} n_e \frac{dT_e}{dt} = \frac{1}{r} \frac{d}{dr} r \left[n_e \chi_e^{HP} \frac{dT_e}{dr} + \frac{5}{2} n_e T_e v_{pinch} \right] + IQ$$

Then v_{pinch} is chosen to nearly cancel the outward heat diffusivity, i.e., $v_{pinch} = -2/5 (\chi_e^{HP} - \chi_e^{PB}) d(\ln T_{e0})/dr$. For typical TFTR parameters $v_{pinch} \sim -1000 r/a$ cm/sec. A problem is that in the perturbed heat equation the heat pinch term is still important, being smaller than the diffusive term only by the factor $(d \ln T_{e0}/dr)/(d \ln T_e/dr) \sim 0.3$. Thus, the heat pulses could look somewhat different than purely diffusive ones. This example is

mathematically equivalent to the previous example where $\tilde{\chi} \sim \alpha (\partial \tilde{T}_e / \partial r) / (\partial T_{e0} / \partial r)$.

A question that arises is that of the origin of the hypothesized $\tilde{\chi}_e(r,t)$. It might be expected that χ_e is caused by enhanced magnetic or electrostatic fluctuations associated with a mode which is destabilized by the crash of the sawtooth. Unfortunately, there are no diagnostics on TFTR at present which have looked for electrostatic fluctuations of this type. The Mirnov loops, which have the time resolution to see magnetic fluctuations at the edge of the plasma have occasionally seen low level (≤ 0.2 Gauss), coherent fluctuations (~ 6 kHz) persisting for one to two milliseconds following the crash of a sawtooth. As $\tilde{\chi}_e$ should have a strong radial dependence, approaching zero at the wall, internal measurements of turbulence levels where $\tilde{\chi}_e$ is largest are necessary to address this question.

In summary, we have shown that sawtooth-induced electron temperature perturbations diffuse through the TFTR plasma at a rate which is faster than that expected from the overall equilibrium electron heat transport (i.e., $\chi_e^{HP} \gg \chi_e^{PB}$). While we have shown conclusively that the heat pulse propagation is diffusive [i.e., describable by Eq. (2) and not ballistic], we do not have a viable model to explain why $\chi_e^{HP} \gg \chi_e^{PB}$. Resolution of this discrepancy could shed considerable light on the anomalous transport mechanisms operative in large tokamak plasmas such as TFTR.

ACKNOWLEDGMENTS

This work was supported by U.S. Dept. of Energy Contract No. DE-AC02-76-CHO-3073 and ORNL research was sponsored by the Office of Fusion Energy, U.S. Department of Energy, under contract No. DE-AC05-84OR21400 with Martin Marrietta Energy Systems, Inc.

APPENDIX A

In the analysis leading to the fundamental heat pulse evolution equation, Eq. (2), it is assumed that the sawtooth phenomenon just redistributes the electron temperature profile; i.e., there is no net electron heat input because of the sawtooth. However, there can be heat input from the sawtooth "crash" phase due to the conversion of magnetic energy into thermal energy in the magnetic reconnection phase. In this appendix we show that this extra heat input is usually small, and hence can be neglected.

The total energy in the poloidal magnetic field inside the reconnection radius is given by ($q = rB_T/RB_D$)

$$E_M = \int_0^{r_0} d^3x \frac{B_D^2}{2u_0} = \frac{B_T^2}{2u_0} (2\pi R) \frac{1}{R^2} \int_0^{r_0} 2\pi r dr \left(\frac{r^2}{q^2}\right) \quad (A.1)$$

where r_0 is the reconnection radius.

However, not all of this energy is available for conversion to kinetic energy during the reconnection process. Defining the helical flux for the $m = 1$ modes by ψ with

$$\frac{d\psi}{dr} = \left(\frac{1}{q} - 1\right)r, \quad (A.2)$$

we can write

$$\frac{r}{q} = r + \frac{d\psi}{dr}. \quad (A.3)$$

Utilizing this in Eq. (A.1) we can identify the amount of magnetic energy available from reconnection as that due to rearrangement of the helical flux, hence, the magnetic energy available is given by

$$E_A = \frac{B_T^2}{2\mu_0} (2\pi R) \frac{1}{R^2} \int_0^{r_0} 2\pi r dr \left(\frac{d\psi}{dr}\right)^2. \quad (\text{A.4})$$

Note that E_A is an upper bound on the energy released during a reconnection, assuming that ψ is conserved and following Kadomtsev¹¹ the actual energy released is of order half of E_A .

The ratio of this energy to the kinetic energy of the electron plasma component inside the radius r_0 is (assuming for simplicity that n and T are nearly constant in radius)

$$\begin{aligned} E_A/E_{th} &= E_A / (2\pi R \int_0^{r_0} 2\pi r dr n_e T_e) \\ &= \frac{1}{\beta_p} \frac{1}{\pi r_0^4} \int_0^{r_0} 2\pi r dr \left(\frac{d\psi}{dr}\right)^2 \equiv \frac{I_*}{\beta_p}, \end{aligned} \quad (\text{A.5})$$

in which $\beta_p \equiv n_e T_e / (B_p^2 / 2\mu_0)$ the plasma poloidal β at the position $r = r_0$, and the dimensionless integral I_* is defined by

$$I_* \equiv \frac{2}{r_0^4} \int_0^{r_0} r dr \left(\frac{d\psi}{dr}\right)^2. \quad (\text{A.6})$$

In order to evaluate this we need a specific model for $q(r)$. Taking the analytically convenient profile

$$q(r) = q_0 (1 + (r/r_0)^{2p})^{1/p},$$

we find for $r_s/r_p = 0.4$ and $q(\text{wall}) = 2.8$ the values indicated in Table A.1 below.

Table A.1

Approximate values of the dimensionless integral

I_* for various values of q_0

q_0	0.6	0.8	0.9	0.98
p	0.9	1.4	2	3.4
I_*	0.033	0.01	0.005	0.0004

From numerical simulations of the very slow resistive diffusion of the current profile on axis after a sawtooth "crash" one typically finds $q_0 = 0.93 - 0.999$. Thus, we would expect $I_* < 10^{-2}$ and hence for typical values of $\beta_p \sim 0.3$, the kinetic energy added to the plasma through magnetic reconnection would typically be a few percent or less, and hence be negligible.

REFERENCES

- [1] P.C. EFTHIMION et al., Phys. Rev. Lett. 52, (1984) 1492.
- [2] E. EJIMA and M. OKABAYASHI, Phys. Fluids 8, (1975) 904.
- [3] J.D. CALLEN and G.L. JAHNS, Phys. Rev. Lett. 38, (1977) 971.
- [4] G.L. JAHNS, M. SOLER, B.V. WADDELL, J.D. CALLEN, and H.R. HICKS, Nucl. Fusion 18, (1978) 609.
- [5] M. SOLER and J.D. CALLEN, Nucl. Fusion 19, (1979) 703.
- [6] J.D. BELL et al., Nucl. Fusion 24, (1984) 997.
- [7] D. SWAIN et al., Nucl. Fusion 21, (1981) 1409.
- [8] G.L. JAHNS, S.K. Wong, R. PRATER, S.H. LIN, and S. EJIMA, "Measurement of Thermal Transport by Synchronous Detection of Modulated Electron Cyclotron Heating in the Doublet III Tokamak," GA Technologies Report GA-A17858, February 1985.
- [9] H.S. CARSLAW and J.C. JAEGER, Conduction of Heat Solids, 2nd Ed. (Oxford Univ. Press, N.Y., 1959).
- [10] This possibility was suggested to the authors by R. J. Hawryluk.
- [11] B.B. Kadomtsev, Fizica Plazmy 1, (1975) 710.

Table I

Average values of $x_e(r)$ from t_p versus r^2 in Fig. 10

Case	<u>1</u>	<u>2</u>	<u>3</u>	<u>4</u>	<u>5</u>	<u>6</u>
r^2/a^2 fitted	0.1/0.6	0.1/0.4	0.1/0.4	0.1/0.4	0.1/0.34	0.1/0.34
\bar{x}	1	3	3	3	2.7	0.83
$x_e^{HP} \equiv (r_2^2 - r_1^2)/8t_p$	1	2.9	2.7	2.5	2.1	1

FIGURE CAPTIONS

- FIG. 1. Schematic illustration of soft X-ray diagnostic chords and the electron temperature perturbation evolution $T(r,t)$ as a function of time. The signals below indicate the temporal variation of the soft X-ray signals from the various chords (1-5). At later times $t_2 > t_1 > t_0$ the sawtooth-induced heat pulse diffuses radially outward from the radius r_0 to which reconnection (flattening of T_e) takes place.
- FIG. 2. Soft X-ray signals from lower chords illustrating the sawtooth crash in the center and the propagation of the heat pulse outwards. The various signals are labeled by the minimum tangency radius. (Typical sawtooth, $I_p = 1.0$ MA, $\bar{n} = 1.2 \times 10^{13}/\text{cm}^3$, $a = 83$ cm, $q_a = 3.6$, $\chi_e^{\text{PB}} = 0.9 \cdot 10^4$ cm²/sec.)
- FIG. 3. Soft X-ray signals from selected chords illustrating the sawtooth crash in the center and slow outward propagation of the "inverted sawtooth" heat pulse. The various signals are labeled by the minimum tangency radius (> 0 above midplane, < 0 below midplane) of the soft X-ray chord. (Event sawtooth, $I_p = 1.1$ MA, $\bar{n} = 2.1 \times 10^{13}/\text{cm}^3$, $a = 83$ cm, $q_a = 3.2$, 500 Hz sampling rate.)
- FIG. 4. Illustrative plot of t_p versus r^2 to determine χ_e . [Normal (solid) and event (dashed) sawteeth, same parameters as Figs. 2 and 3, soft X-rays.]

FIG. 5. Comparison of temperature perturbation measured from ECE spectrometer at $r = 47$ cm ($R = 208$ cm) with the predicted temporal behavior from Eq. (7). ($I = 1.4$ MA, $\bar{n} = 3 \times 10^{13}/\text{cm}^3$, $a = 83$ cm, $q_a = 2.6$, $r_s = 35$ cm, $t_p \approx 5$ msec, $\chi_e^{\text{HP}} \approx 2.3 \times 10^4$ cm²/sec, $\chi_e^{\text{PB}} \approx 1.1 \cdot 10^4$ cm²/sec, 4 msec sampling time interval.)

FIG. 6. Definition of the times for the electron temperature heat pulse to reach its maximum, 0.75, 0.5, and 0.25 fractions of the peak temperature perturbation.

FIG. 7. Illustrative plot of $t_{0.5}$ versus r^2 to determine χ_e from soft X-ray and ECE data. (Same parameters as Fig. 5.)

FIG. 8. Comparison of maximum (in time) temperature perturbation due to heat pulse propagation with the theoretically predicted scaling of r^{-4} . (Same parameters as Fig. 5, ECE measurement of T_e .)

FIG. 9. Example of the radial increase of the phase shift of the first Fourier harmonic of the heat pulses, from which an electron heat diffusivity $\chi_e^{\text{HP}} \approx 4 \cdot 10^4$ cm²/sec can be inferred. (Same parameters as Fig. 2.)

FIG. 10. χ_e^{HP} versus minor radius determined from data in Fig. 9. The error bars are determined by analyzing subsets of the data.

FIG. 11. Example of the radial increase of the phase shifts of the first three Fourier harmonics of the heat pulses from which the electron heat diffusivity χ_e^{HP} is inferred to be 4.1, 4.0, and $4.3 \cdot 10^4$ cm^2/sec , respectively, $\chi_e^{\text{PB}} = 0.7 \cdot 10^4$ cm^2/sec . TFTR. n indicates the harmonic number of the basic frequency $\omega = 2\pi/\tau_{\text{saw}}$.

FIG. 12. Estimate of initial condition $\Delta T_e(r)$ derived from change in ECE measured electron temperature profile from before to after the sawtooth "crash." The scale length δr indicates the radial uncertainty in the data brought about by the finite radial heat transport occurring during the roughly 1.2 msec crash phase of the sawtooth ($\Delta r \sim \sqrt{4\chi\delta t}$). Also, it should be noted that the ECE profile data are obtained with a 4 ms sweep time, and the sawtooth crash occurs during one sweep. (Same parameters as Fig. 5.)

FIG. 13. Slight variation of the numerically calculated time of the peak of the heat pulse versus r^2 for various initial conditions ($n = \text{constant}$, $\chi_e = \text{constant}$). Here, and in Figs. 14 and 15, Δr^2 is defined as $r^2 - r_0^2$ where r_0 is the reconnection radius.

FIG. 14. Slight variation of the numerically calculated time of the peak of the heat pulse versus r^2 for various density profiles ($\chi_e = \text{constant}$).

FIG. 15. Variation of the numerically calculated arrival time of the peak of the heat pulse versus r^2 for various $n(r)$ and $\chi_e(r)$ profiles.

FIG. 16. Calculation of the arrival time of the peak of the heat pulse versus r^2 from the HEATX code⁶ for multiple pulses (0 - 6 $\rightarrow \infty$). For these calculations $\chi_e = 8 \times 10^3 \text{ cm}^2/\text{sec}$, $\tau_{\text{saw}} = 25 \text{ msec}$.

FIG. 17. Comparison of χ_e 's determined by phase shift analysis of heat pulse propagation with those determined from power balance.

FIG. 18. Example of increasing propagation speed of heat pulses from the event through successive sawteeth in TFTR. ($I = 1.4 \text{ MA}$, $\bar{n} = 3.1 \times 10^{13}/\text{cm}^3$, $a = 83 \text{ cm}$, $q_a = 3.6$.)

FIG. 19. TFTR heat pulses simulated with BALDUR transport code. ($R_0 = 2.55 \text{ m}$, $a = 0.8 \text{ m}$, $B = 4 \text{ T}$, $I = 1.4 \text{ MA}$, $r_s = 25 \text{ cm}$, $r_0 = 33 \text{ cm}$, $r = 35 \text{ cm}$, $\tau_{\text{saw}} = 60 \text{ msec}$, $\chi_e = 5 \times 10^3 \text{ cm}^2/\text{sec}$.)

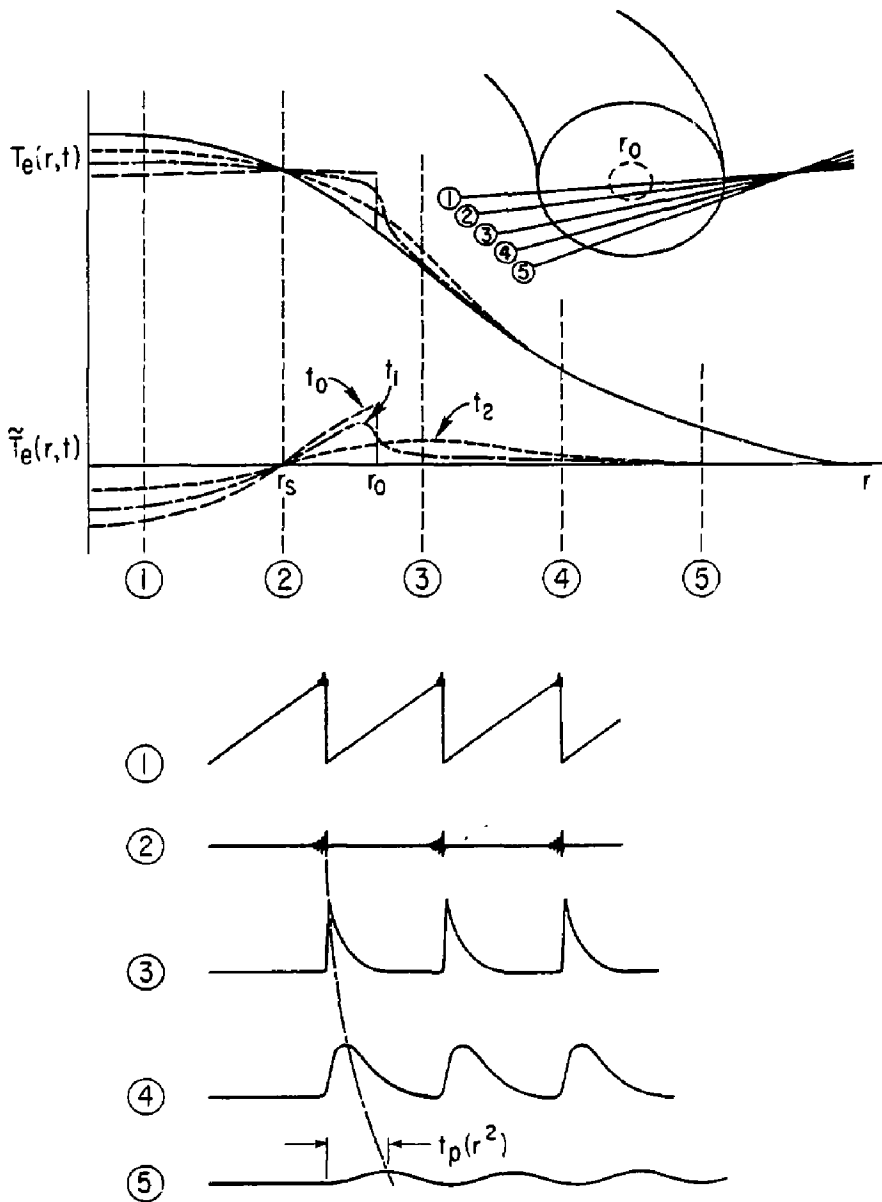


Fig. 1

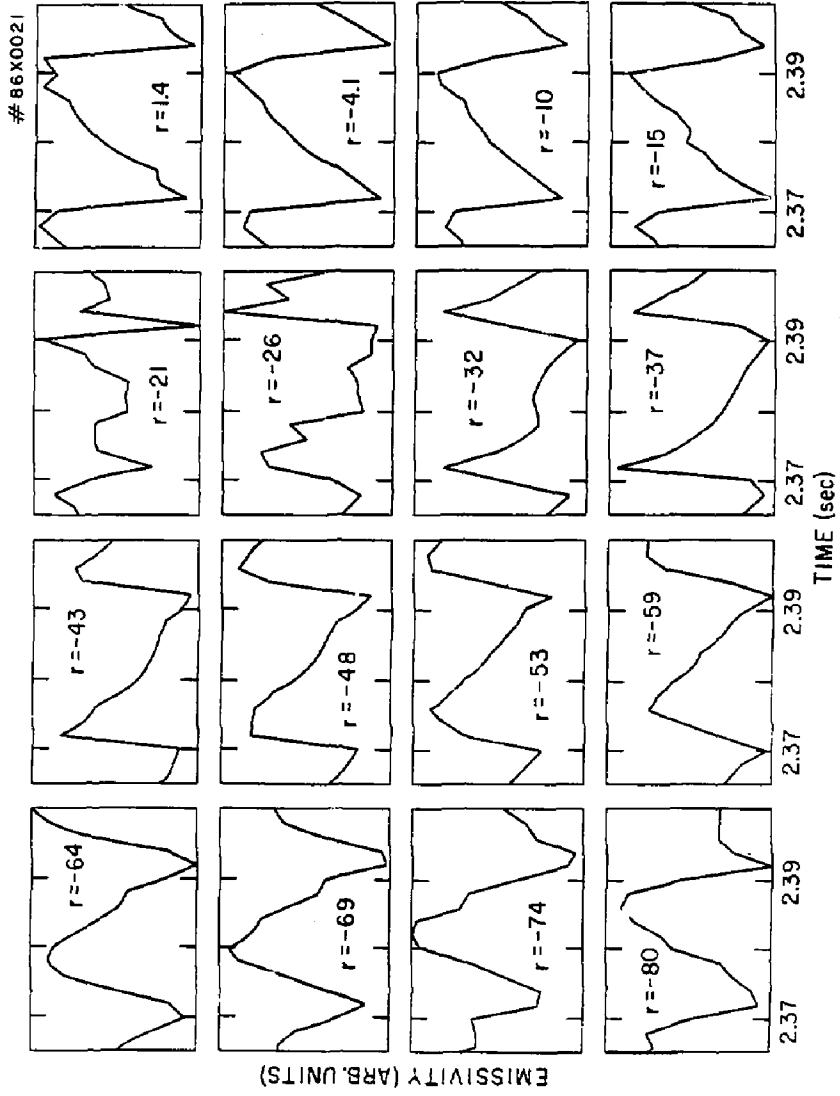


Fig. 2

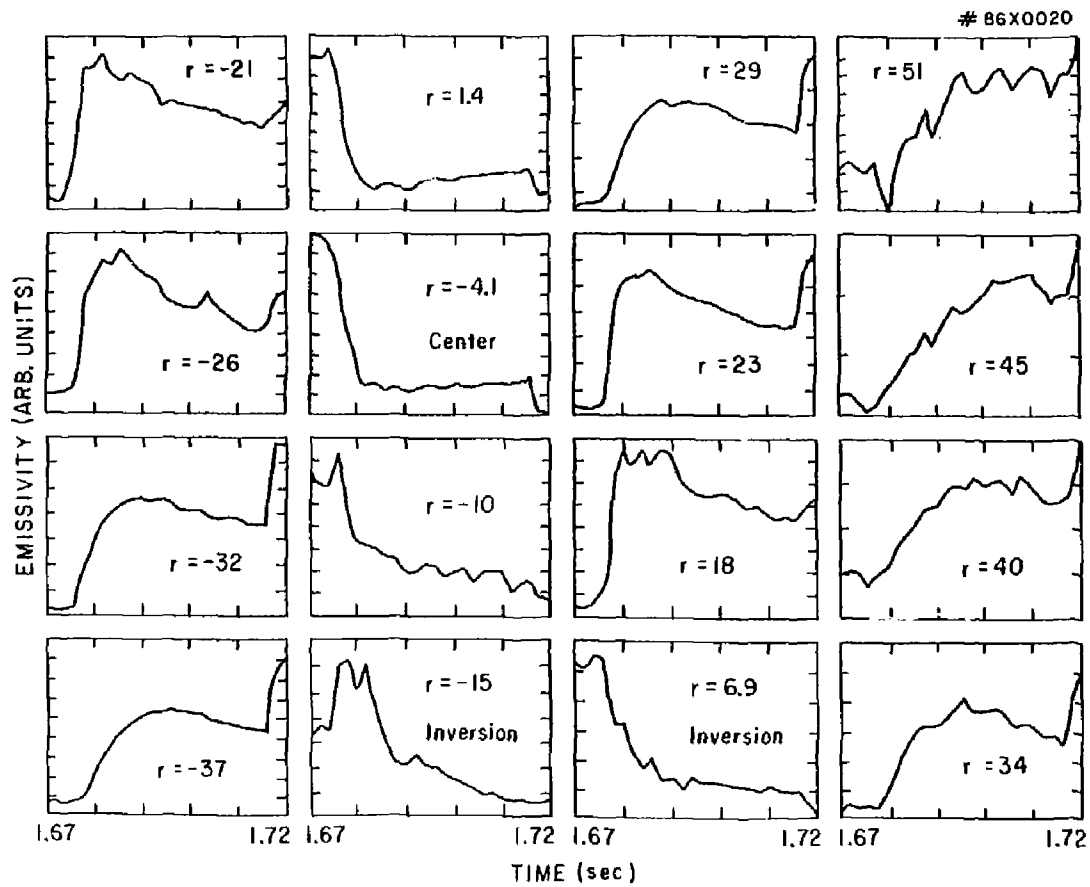


Fig. 3

85X1423

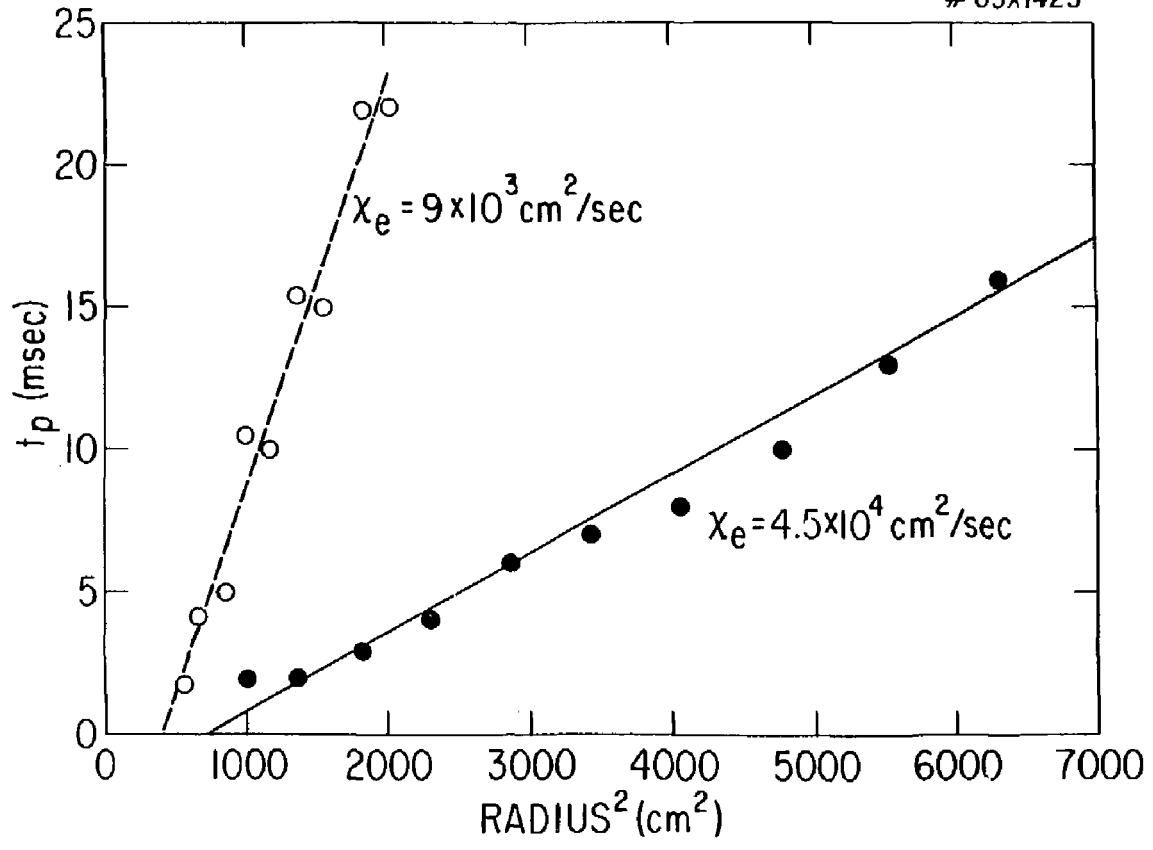


Fig. 4

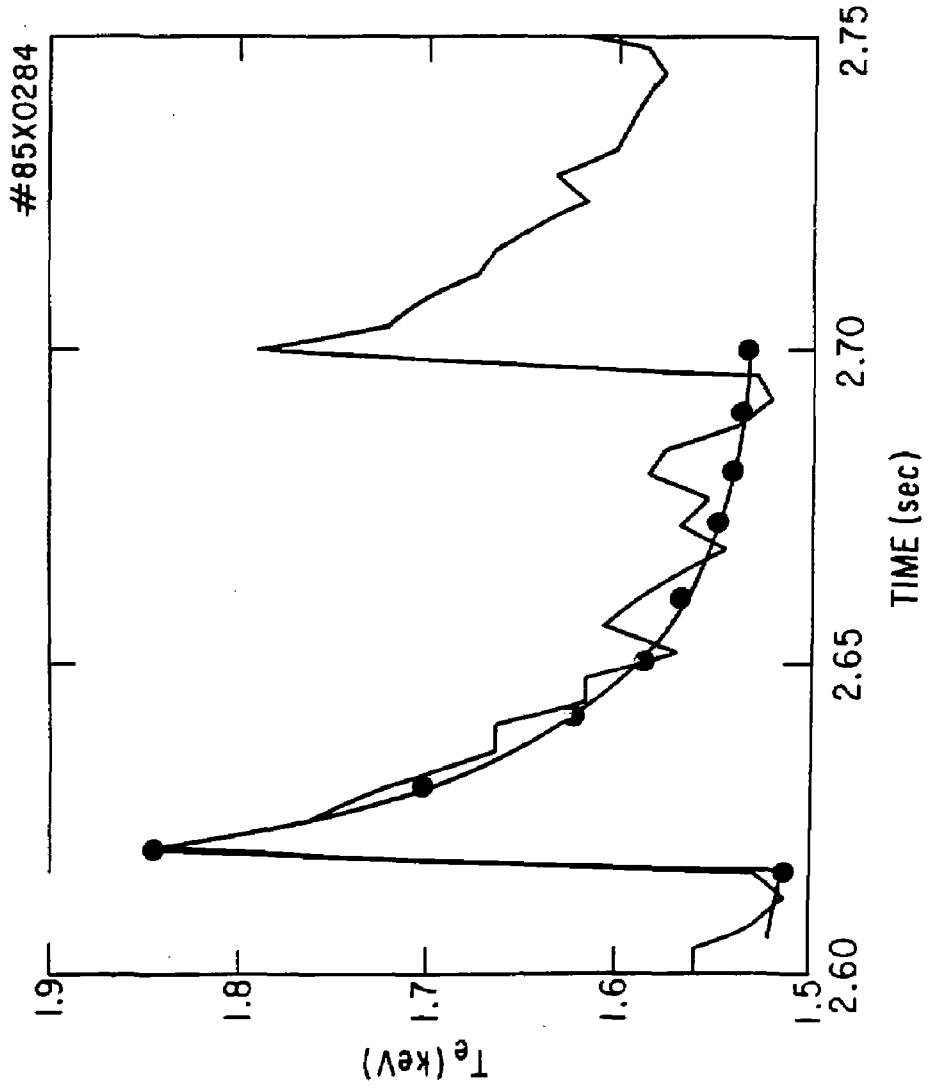


Fig. 5

#85X0550

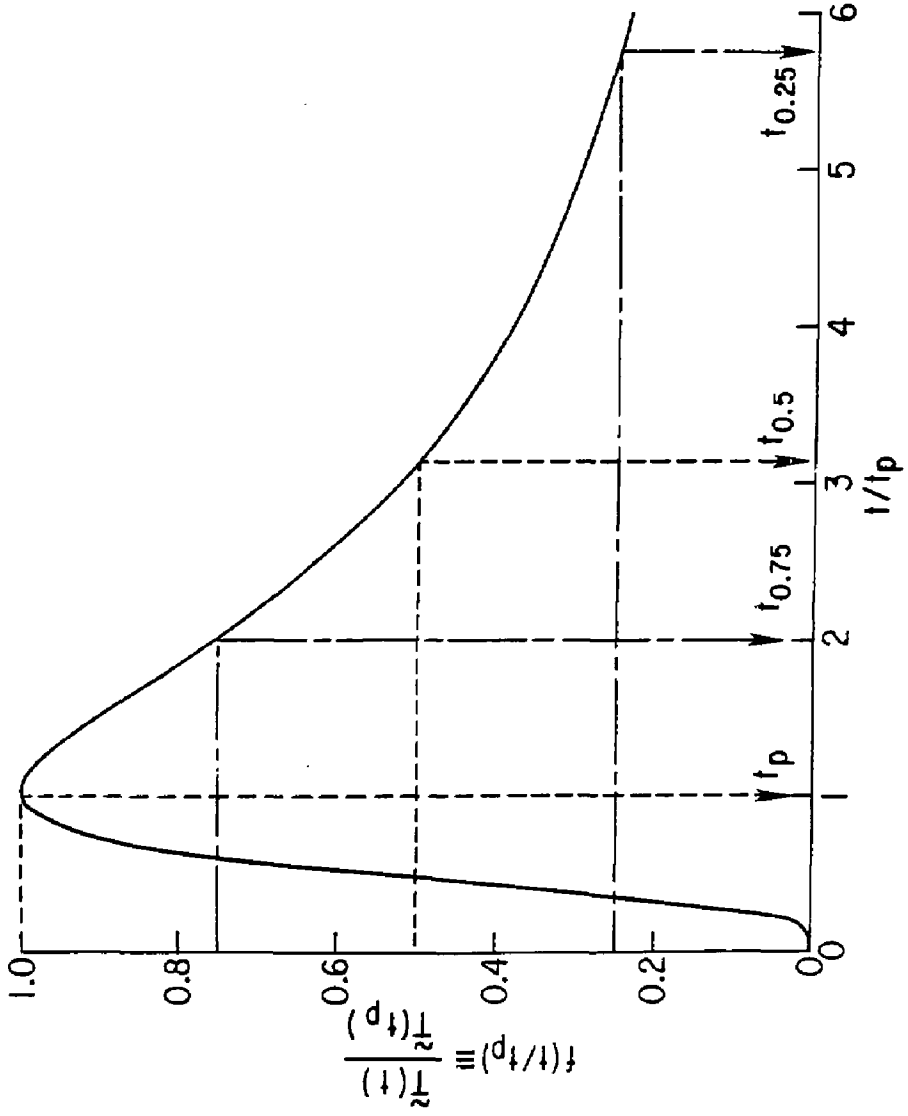


Fig. 6

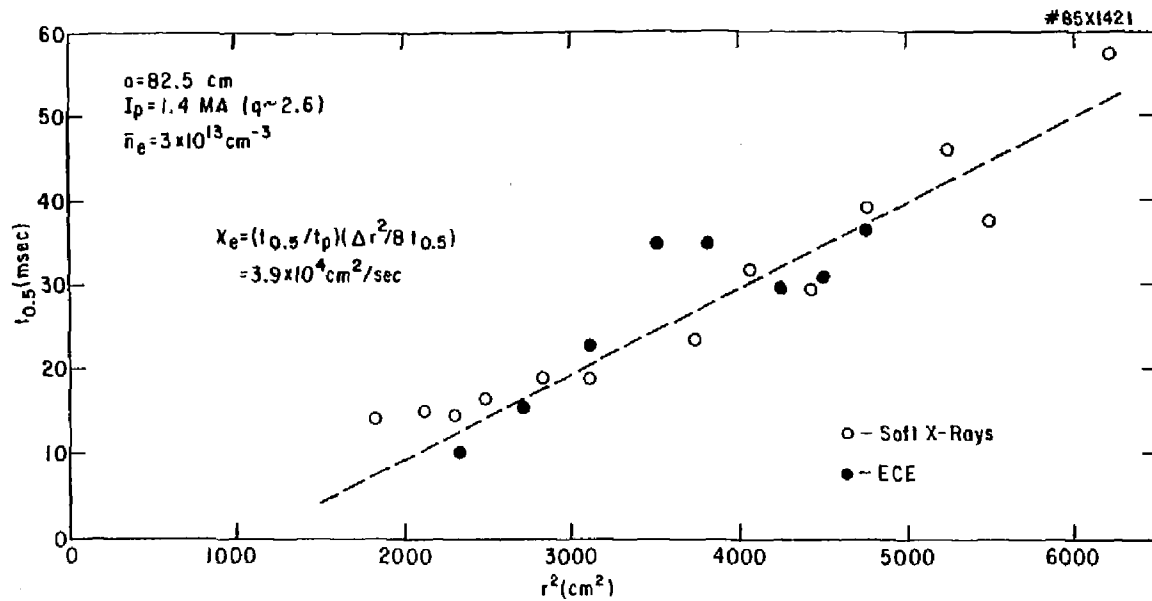


Fig. 7

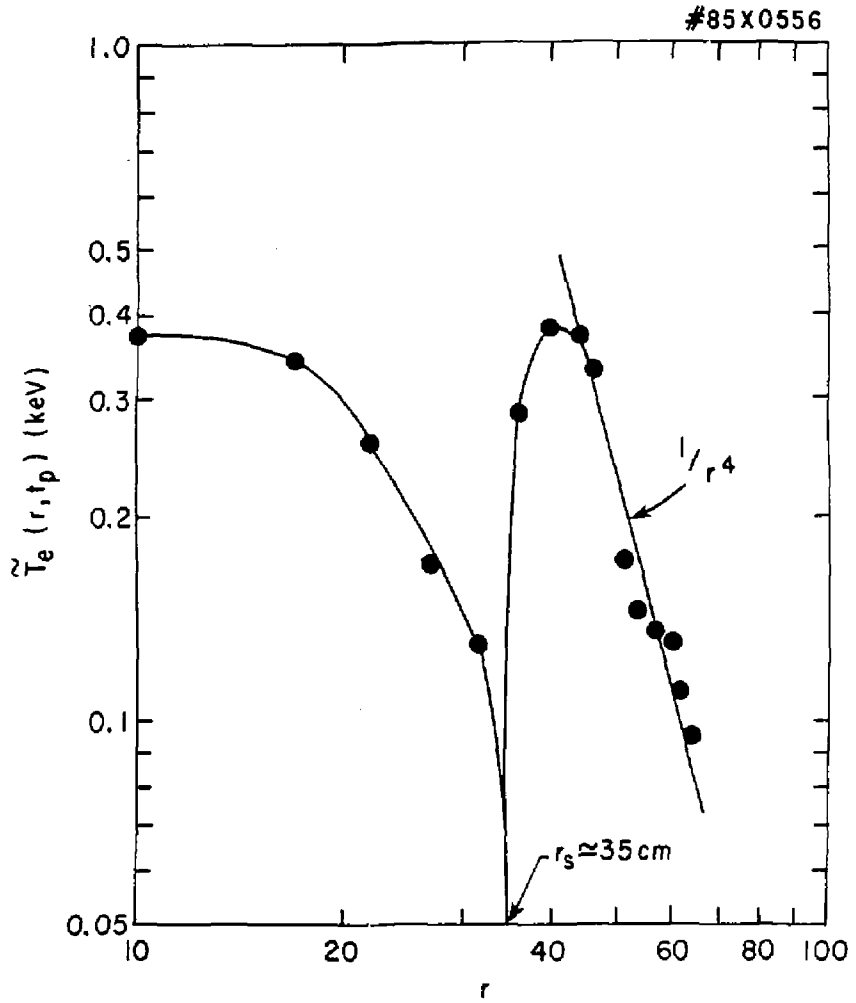
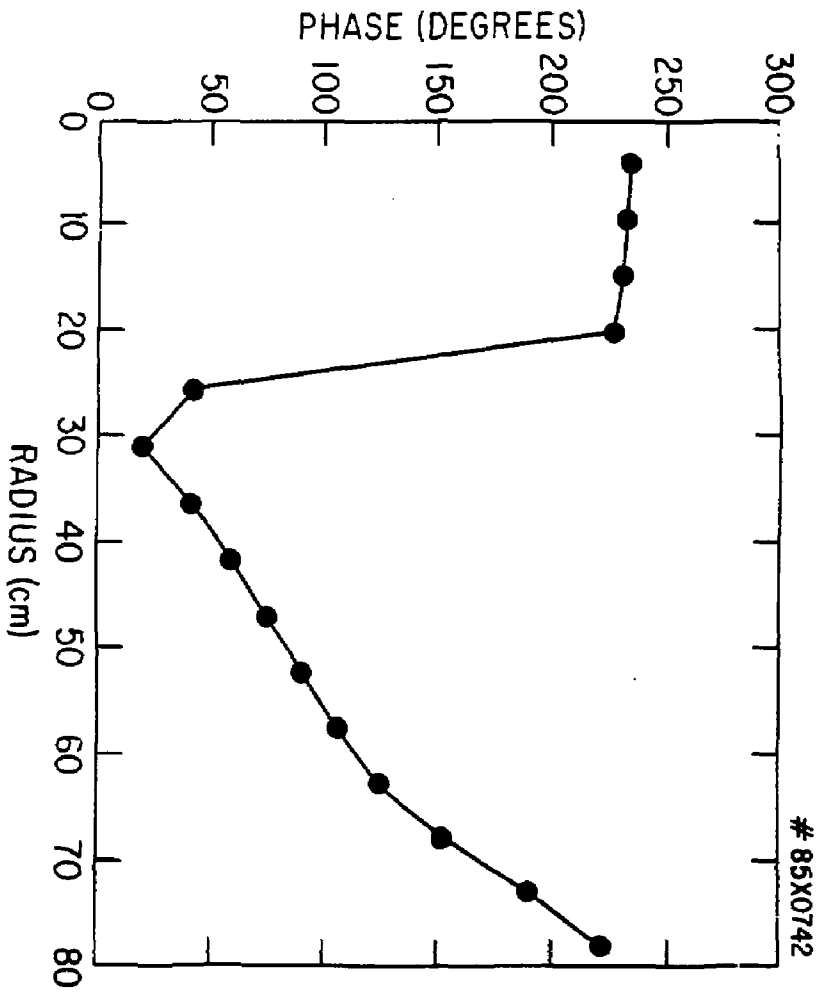


Fig. 2



85X0742

Fig. 9

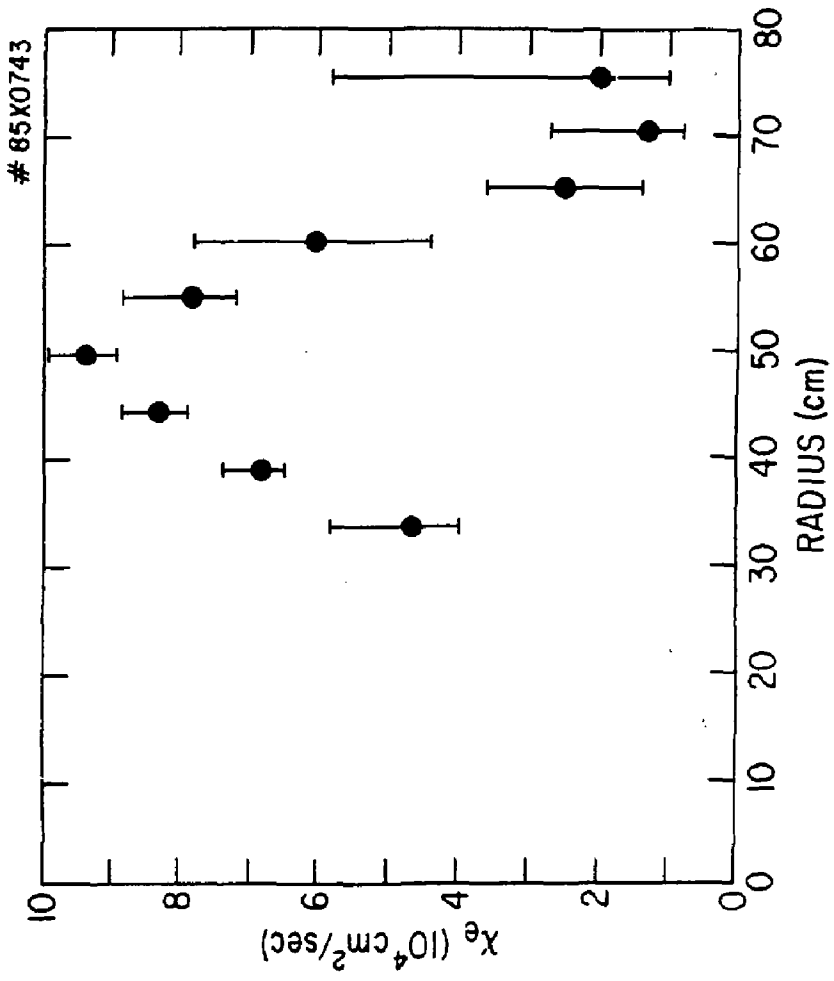


Fig. 10

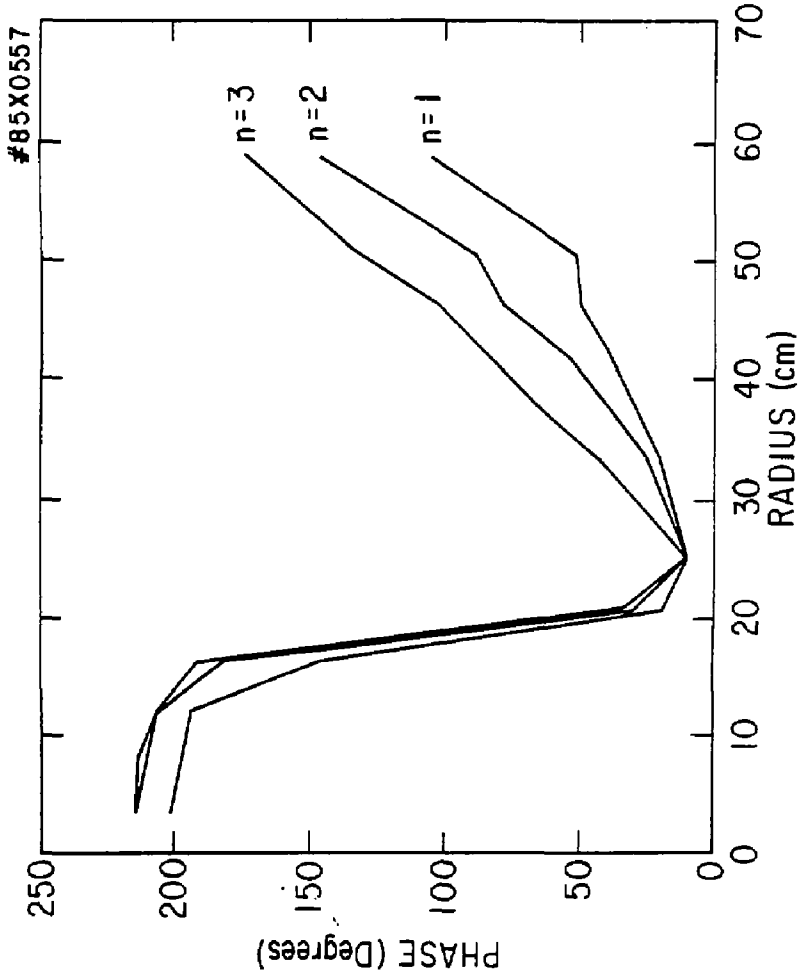


Fig. 11

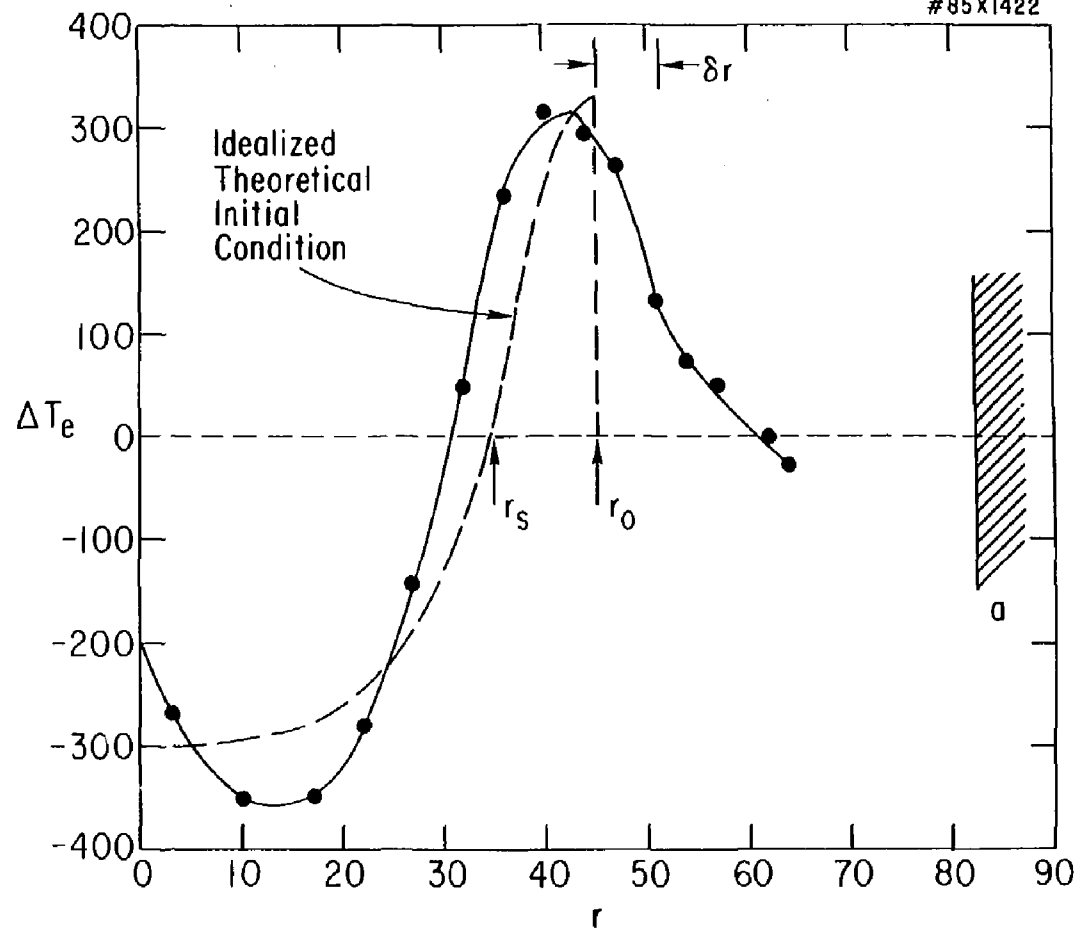


Fig. 12

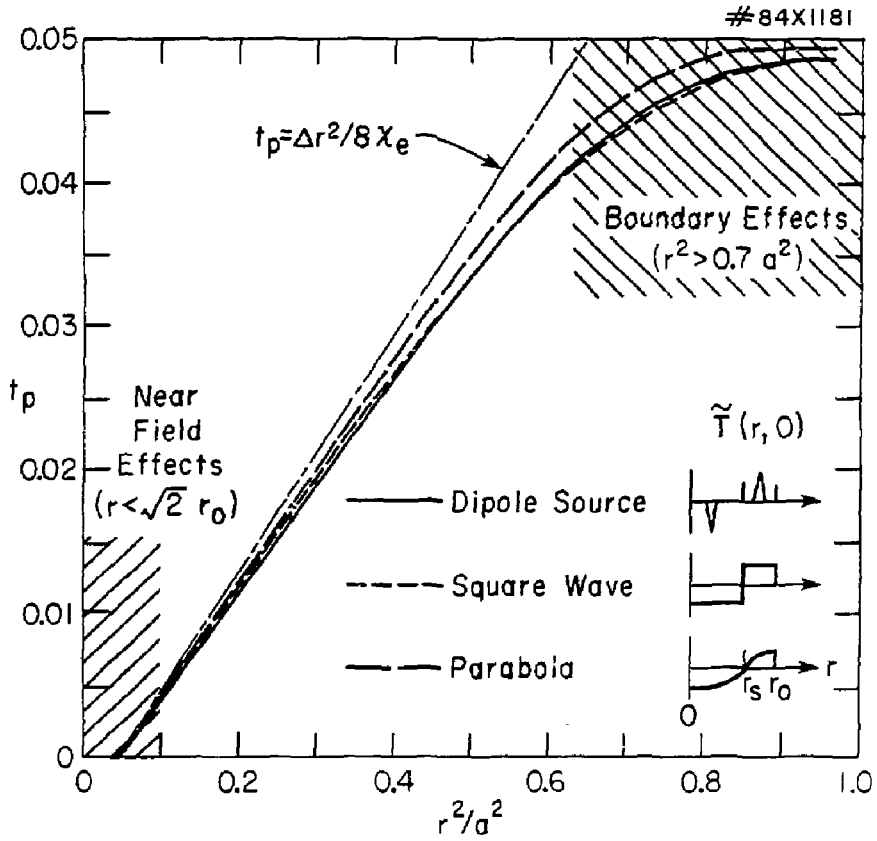


Fig. 13

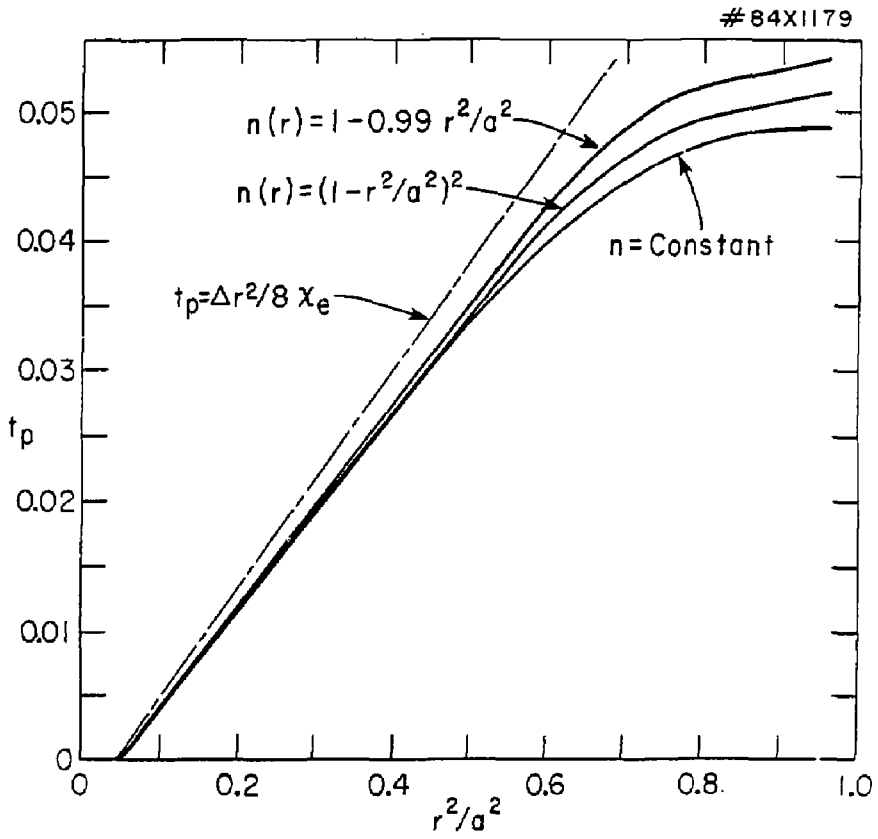


FIG. 14

#85X0283

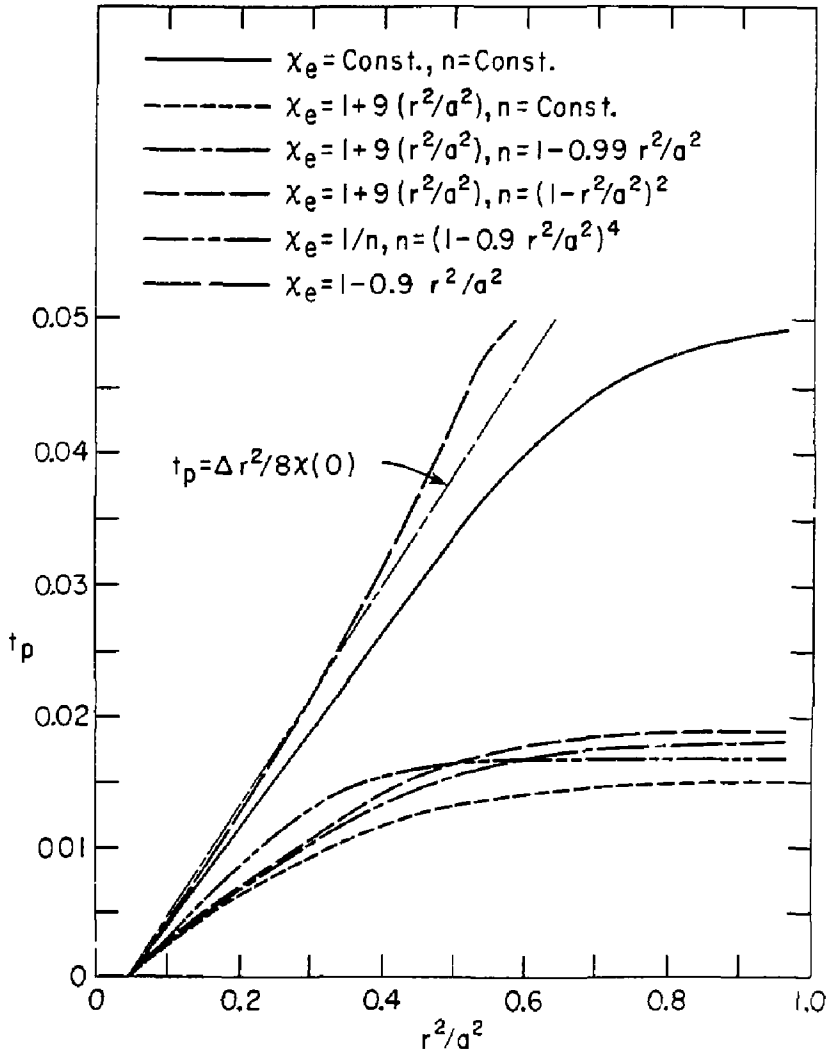


Fig. 15

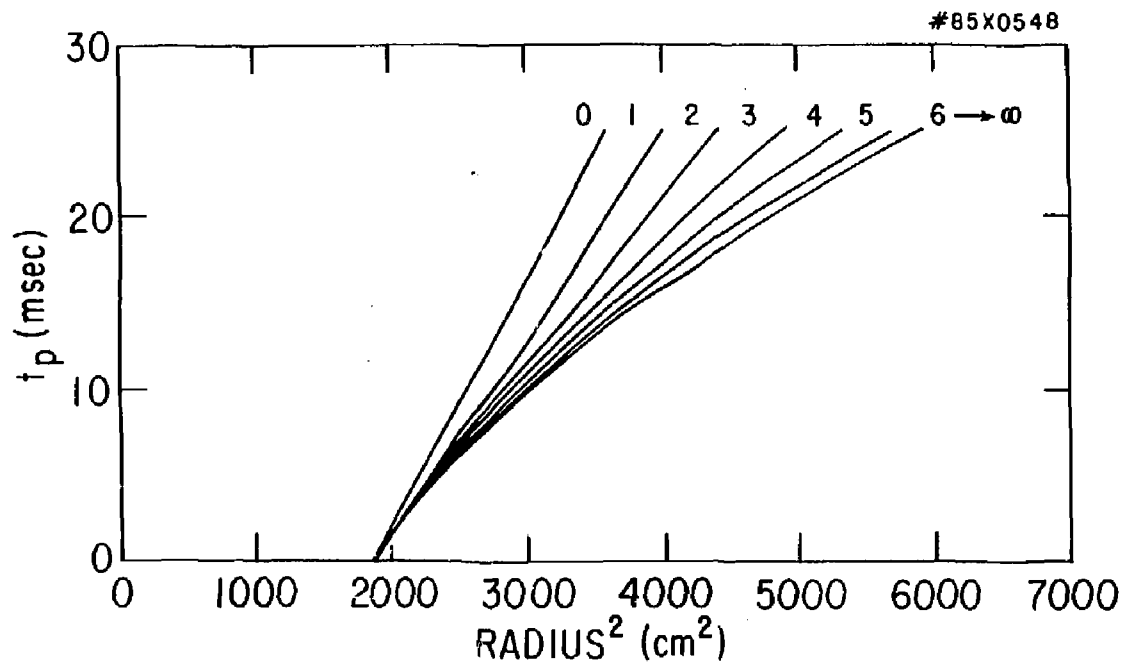


Fig. 16

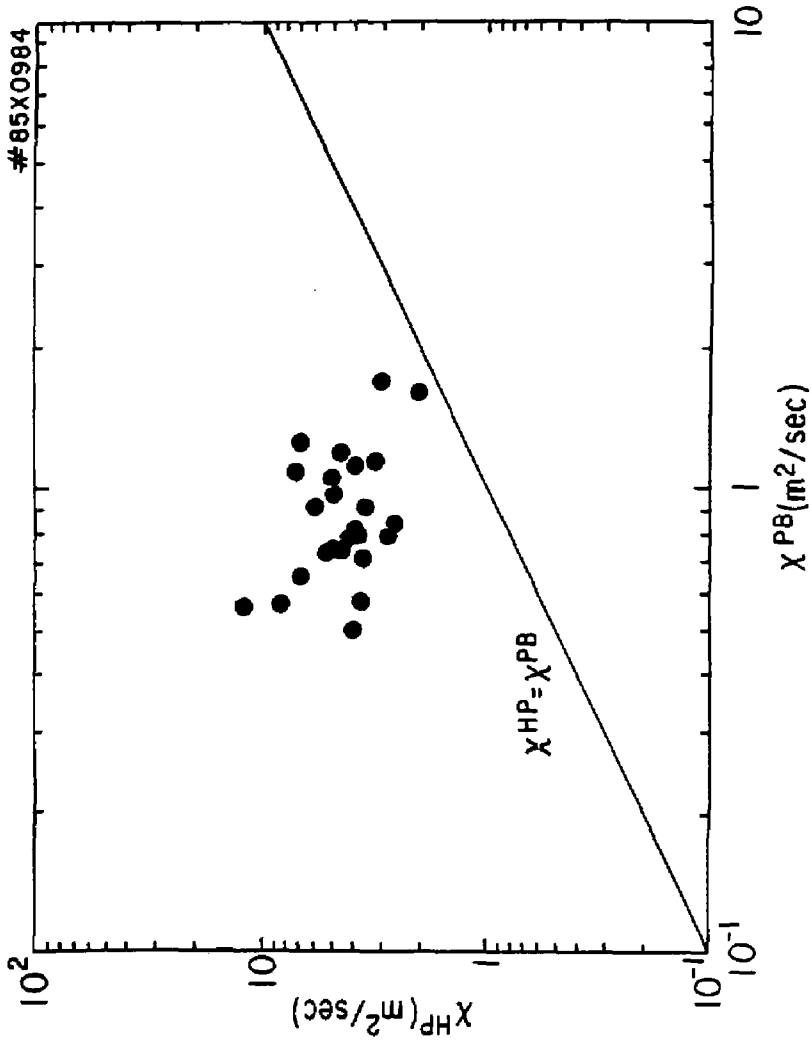


Fig. 17

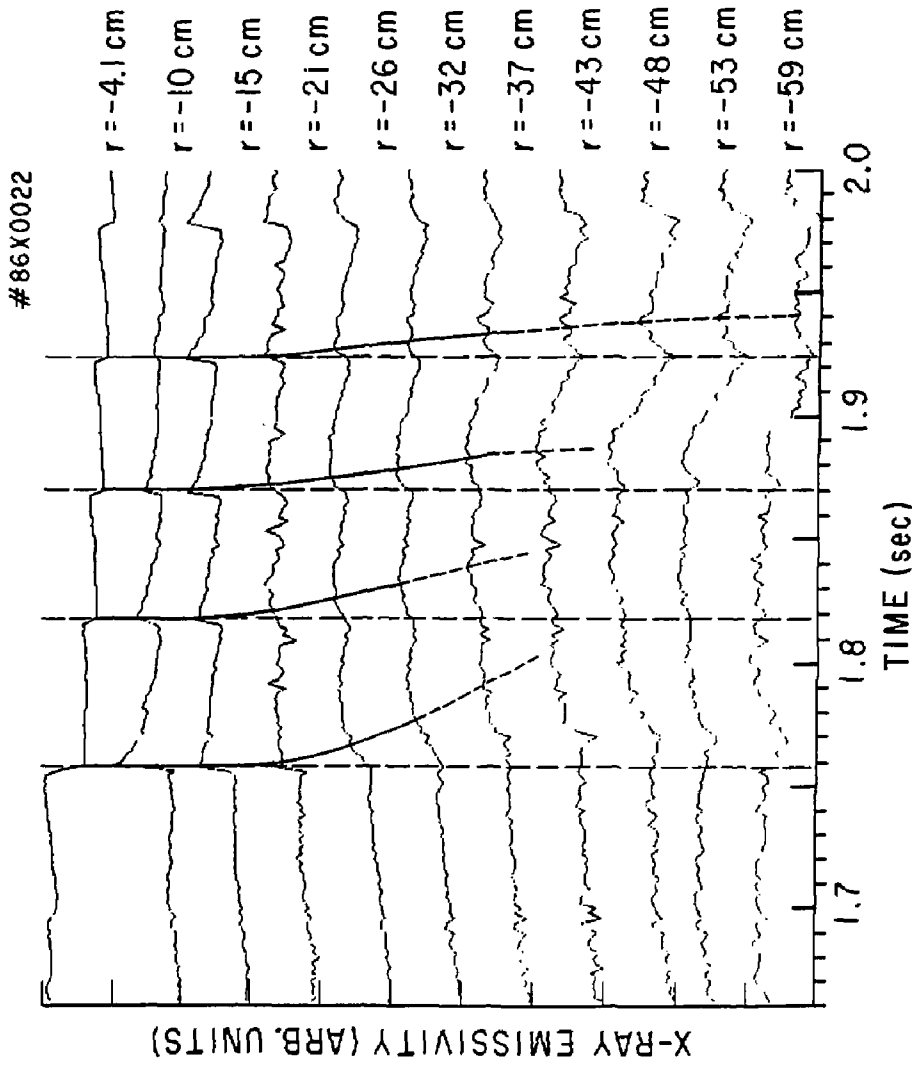


Fig. 18

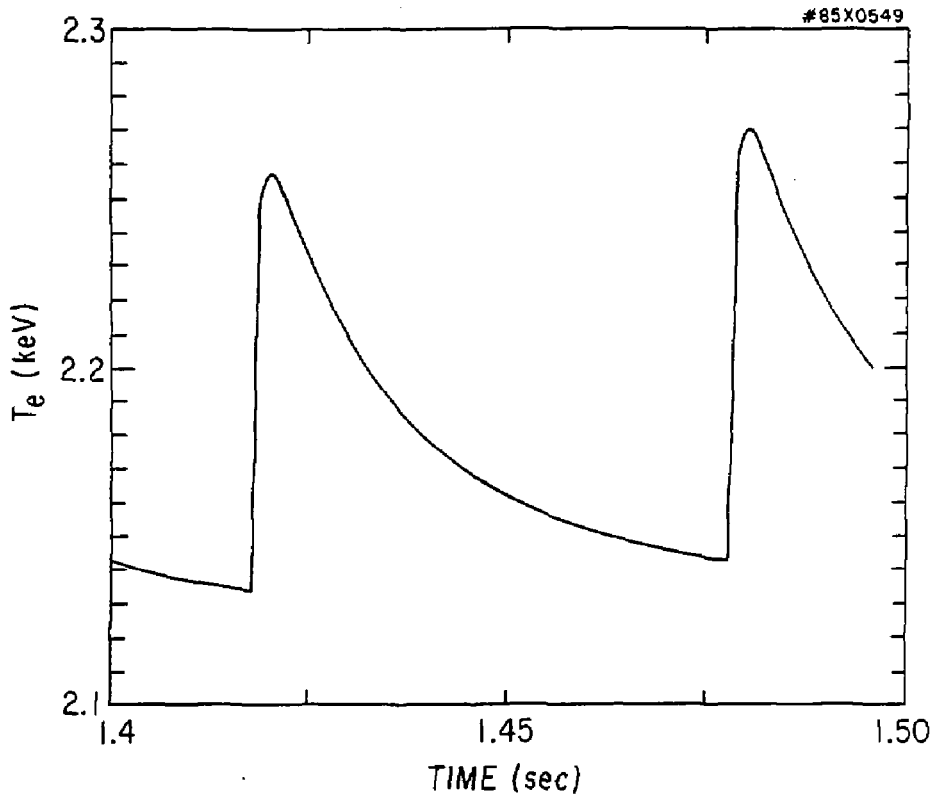


Fig. 19

EXTERNAL DISTRIBUTION IN ADDITION TO UC-20

Plasma Res Lab, Ausstra Nat'l Univ, AUSTRALIA
Dr. Frank J. Paoloni, Univ of Wollongong, AUSTRALIA
Prof. I.R. Jones, Flinders Univ., AUSTRALIA
Prof. M.H. Brennan, Univ Sydney, AUSTRALIA
Prof. F. Cag, Inst Theo Phys, AUSTRIA
Prof. Frank Verheest, Inst theoretische, BELGIUM
Dr. D. Palumbo, Dg XII Fusion Prog, BELGIUM
Ecole Royale Militaire, Lab de Phys Plasmas, BELGIUM
Dr. P.H. Sakaraka, Univ Estadual, BRAZIL
Dr. C.R. James, Univ of Alberta, CANADA
Prof. J. Teichner, Univ of Montreal, CANADA
Dr. H.M. Skarsgard, Univ of Saskatchewan, CANADA
Prof. S.R. Sreenivasan, University of Calgary, CANADA
Prof. Tudor W. Johnston, INRS-Energie, CANADA
Dr. Hannes Barnard, Univ British Columbia, CANADA
Dr. M.P. Sadynski, MPI Technologies, Inc., CANADA
Chalk River, Nucl Lab, CANADA
Zhengxi Li, SW Inst Physics, CHINA
Library, Tsing Hua University, CHINA
Librarian, Institute of Physics, CHINA
Inst Plasma Phys, Academia Sinica, CHINA
Dr. Peter Lukac, Komenského Univ, CZECHOSLOVAKIA
The Librarian, Culham Laboratory, ENGLAND
Prof. Schatzman, Observatoire de Nice, FRANCE
J. Radet, CEN-SP6, FRANCE
AM Dupas Library, AM Dupas Library, FRANCE
Dr. Tom Mual, Academy Bibliographic, HONG KONG
Preprint Library, Cent Res Inst Phys, HUNGARY
Dr. R.K. Chhajlani, Vikram Univ, INDIA
Dr. B. Dasgupta, Saha Inst, INDIA
Dr. P. Kaw, Physical Research Lab, INDIA
Dr. Phillip Rosenau, Israel Inst Tech, ISRAEL
Prof. S. Cuperman, Tel Aviv University, ISRAEL
Prof. G. Rostaqni, Univ Di Padova, ITALY
Librarian, Int'l Ctr Theo Phys, ITALY
Miss Clelia De Palo, Assoc EURATOM-ENEA, ITALY
Biblioteca, del CNR EURATOM, ITALY
Dr. H. Yamato, Toshiba Res & Dev, JAPAN
Direc. Dept. Lj, Tokamak Dev, JAERI, JAPAN
Prof. Nobuyuki Inoue, University of Tokyo, JAPAN
Research Info Center, Nagoya University, JAPAN
Prof. Kyoji Nishikawa, Univ of Hiroshima, JAPAN
Prof. Sigeru Mori, JAERI, JAPAN
Prof. S. Tanaka, Kyoto University, JAPAN
Library, Kyoto University, JAPAN
Prof. Ichiro Kawakami, Nihon Univ, JAPAN
Prof. Satoshi Itoh, Kyushu University, JAPAN
Dr. D.I. Choi, Adv. Inst Sci & Tech, KOREA
Tech Info Division, KAERI, KOREA
Bibliothek, Kon-Inst Voor Plasma, NEETHERLANDS
Prof. B.S. Lilley, University of Waikato, NEW ZEALAND
Prof. J.A.C. Cabral, Inst Superior Techn, PORTUGAL
Dr. Octavian Petrus, ALI CUZA University, ROMANIA
Prof. M.A. Hellberg, University of Natal, SO AFRICA
Dr. Johan de Villiers, Plasma Physics, Micoor, SO AFRICA
Fusion Div. Library, JEN, SPAIN
Prof. Hans Wilhelmson, Chalmers Univ Tech, SWEDEN
Dr. Lennart Stenflo, University of UMEA, SWEDEN
Library, Royal Inst Tech, SWEDEN
Centre de Recherchesen, Ecole Polytech Fed, SWITZERLAND
Dr. V.T. Tolok, Kharkov Phys Tech Ins, USSR
Dr. D.D. Ryutov, Siberian Acad Sci, USSR
Dr. G.A. Eliseev, Kurchatov Institute, USSR
Dr. V.A. Glukhikh, Inst Electro-Physical, USSR
Institute Gen. Physics, USSR
Prof. T.J.M. Boyd, Univ College N Wales, WALES
Dr. K. Schindler, Ruhr Universitat, W. GERMANY
Nuclear Res Estab, Julich Ltd, W. GERMANY
Librarian, Max-Planck Institut, W. GERMANY
Bibliothek, Inst Plasmaforschung, W. GERMANY
Prof. R.K. Janev, Inst Phys, YUGOSLAVIA